Constructive interaction in an array of flexible energy-harvesting plates in oscillatory cross flow

Qiang Zhu *
Department of Structural Engineering, University of California, San Diego, La Jolla, California 92093-0085, USA

(Received 25 April 2024; accepted 21 June 2024; published 8 July 2024)

The dynamics and energy-harvesting capacity of fixed-free plates covered with piezoelectric materials in oscillatory cross flows are investigated numerically by using a coupled fluid-structure-electric model. The focus is on the effect of hydrodynamic interaction within a formation of such plates. Through systematic simulations, it was discovered that at certain combinations of parameters (e.g., plate stiffness, distance between neighboring plates, and Keulegan-Carpenter number), the group-averaged values of plate deformation and power extraction in an array of plates surpass those of a single stand-alone plate. For example, in an array of five plates the group-averaged deformation and power extraction can be increased by 43% and 110% in comparison with a single plate, respectively. Further investigation shows that this phenomenon is determined by the competition between two mechanisms: the shielding mechanism and the wake energy recovery mechanism. Constructive interaction occurs when the latter one outweighs the former one. Parametric studies have also been conducted to identify the region within the parametric space in which constructive interaction can be achieved.

DOI: 10.1103/PhysRevFluids.9.074101

I. INTRODUCTION

In recent years, flow energy harvesters made of flexible materials have attracted much attention due to their advantages in deployability and reduced environmental footprint. In conventional flow energy harvesters such as wind turbines or water turbines, the actual energy extraction islocalized at the rotational axes where generators are installed. This design, however, is not suitable in flexible devices in which the flow-induced deformation is complicated and occurs all over the body [1]. For these devices, distributed energy extraction that covers the whole body or a significant portion of the body appears to be a better option.

One of the simplest designs is a flexible plate that bends under fluid dynamics load. In this design the energy harvesting includes two consecutive processes: the transfer of mechanical energy from the surrounding flow field into mechanical energy in the plate, and the conversion of the mechanical energy in the plate into electricity.

The first process is essentially flow-induced vibrations of the plate. In most of the existing studies this is achieved by structural instability induced by a steady incoming flow, e.g., the flow-induced oscillation of a flag [2–4], or an inverted flag [5–7] (which is less stable so that it demonstrates more severe responses). To trigger such vibrations, certain conditions about the flow speed and structural properties need to be satisfied.

Compared with flows that are aligned with the elongated structure such as a flag or a plate, cross flows often cause larger bending deformation [8,9]. In such a system, if the incoming flow is steady,

*Contact author: qizhu@ucsd.edu

the structural vibration is caused by unsteady vortex shedding from the structure, which is indirect and not effective. Alternatively, the unsteadiness could also come from the incoming (background) flow itself instead of the physically complicated mechanisms of flow-induced instability or unsteady vortex shedding. For example, in an oscillatory flow field (in nature oscillatory flows are often associated with free-surface waves) there exist time-varying flow speed and time-varying pressure gradient. Flexible plates may harvest both kinetic energy from the flow and potential energy from the pressure gradient, and transfer them into mechanical energy in the structure [10–13].

A popular method to convert the mechanical energy in these plates into electricity is by using attached piezoelectric pairs [14–16]. When deformed, these pieces generate electric voltage. For example, if a single pair of piezoelectric material is attached to each side of the plate, as the plate bends the piece on one side will be stretched, whereas the one on the other side will be compressed. This creates a difference in the voltage they generate so that an electric current can be induced in a circuit connected to these two pieces [6,17]. This design, however, comes across issues when there are points of inflection on the plate where the direction of curvature switches. When this occurs, segments of the plate with opposite signs of the curvature will offset each other and diminish production of electricity. To avoid this shortcoming, it is possible to use multiple pairs of piezoelectric pieces that are distributed along the plate so that the electricity generation is achieved through the local curvature rather than its integrated effect along the chord [18–23].

In a recent study we have examined the energy-harvesting performance of a single piezoelectric plate or a pair of plates from oscillatory cross flows [24]. The dynamics of the system and the energy extraction capacity at different parameters (e.g., flow strength as well as the electric/elastic properties of the piezoelectric plates) have been documented. Among all the findings, the most interesting (and potentially useful) one is the discovery of constructive interactions between two plates in a pair. When this happens, the deformation and energy-harvesting capacity of a plate in the pair surpass those of a single stand-alone plate. This is an indication that this plate is capable of recovering energy from the wake of its neighbor for performance enhancement. There is, however, little knowledge about the exact condition for this to happen. It is not known either whether or not it happens in an array of more than two plates.

For in-depth knowledge of the constructive interactions in an array of piezoelectric plates in oscillatory cross flow, we hereby conduct systematic simulations to predict the dynamics and energy harvesting capacity of such an array with different plate properties (e.g., bending stiffness), configuration (e.g., number of plates in the array and distance between neighboring plates), and ambient flow conditions (e.g., frequency of oscillation and amplitude of flow velocity). Through these simulations we aim at answering the following critical questions: (1) Does constructive interaction occur in an array containing more than two plates? (2) What are the underlying physical mechanisms that contribute to the occurrence of constructive interaction among plates in an array? (3) What are the requirements on the physical parameters for constructive interaction to occur?

The rest of the paper is organized as follows. In the next section we start by describing the physical problem to be studied. This is followed by a brief introduction of the mathematical formulation and the numerical algorithm. The numerical results are then presented. The final section includes conclusions and discussion.

II. PHYSICAL PROBLEM

As shown in Fig. 1, we examine the dynamics of an array of N plates (marked as plate 1 through plate N in the figure). When they are not deformed, these plates are perpendicular to the direction of the background flow. For convenience, we assume that each plate has uniform properties (bending stiffness and mass per unit length) along its length L. They are assumed to be identical to each other. The distance D between neighboring plates is also assumed to be constant. The bottom end of a plate is fixed, while the top end is free. For the purpose of energy harvesting, these plates are covered with continuously distributed pairs of piezoelectric patches [19]. When such a pair is bent following the local deformation of the plate, one side is stretched whereas the other side is

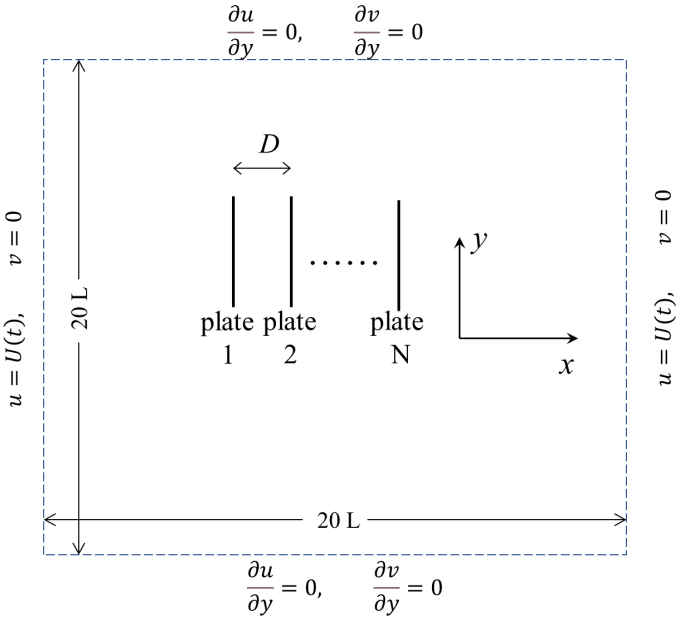

FIG. 1. The computational domain and the boundary conditions.

shortened. This difference in deformation creates an electric voltage between the positive electrodes attached to these two sides. The electrodes are then connected to a purely resistive circuit, where an electric current is induced by the voltage.

The problem is defined within a coordinate system (x, y), with x in the background flow direction (the longitudinal direction) and y in the lateral direction. An oscillatory flow, whose speed varies sinusoidally with time as $U(t) = U_0 \sin(\omega t)$, is applied on the far field. Here U_0 is the amplitude of the flow speed and $\omega = 2\pi/T$ is the frequency (T is the period). This flow condition roughly corresponds to the flow field generated by a shallow-water wave near the bottom, in which there is almost no vertical velocity component. If the wavelength is much larger than the length scale of the system, the variation of the horizontal flow speed in x is negligible.

The study is conducted within a $20L \times 20L$ domain. The boundary conditions for the two velocity components u (in the x direction) and v (in the y direction) are included in Fig. 1.

III. MATHEMATICAL FORMULATIONS AND NUMERICAL APPROACH

A. Governing equations

We assume that the flow is incompressible so that the two-dimensional Navier-Stokes equation is employed for mathematical formulation. We have

$$\rho\left(\frac{\partial \mathbf{u}}{\partial t} + \mathbf{u} \cdot \nabla \mathbf{u}\right) = -\nabla p + \mu \nabla^2 \mathbf{u} + \mathbf{f}(\mathbf{x}, t) \tag{1}$$

and

$$\nabla \cdot u = 0, \tag{2}$$

where $\mathbf{x} \equiv (x, y)$ is the coordinate system shown in Fig. 1. $\mathbf{u} \equiv (u, v)$ is the flow velocity vector. ρ and μ are the density and dynamic viscosity of the fluid, respectively. p is the pressure. $\mathbf{f}$ is the force density exerted by the immersed structure on the fluid.

In the structural part, we first focus on plate 1, whose dynamic responses are governed by

$$m\frac{\partial^2\mathbf{X}}{\partial t^2} = \frac{\partial}{\partial s}(\sigma\boldsymbol{\tau}) - \frac{\partial^2}{\partial s^2}\left(k_b\frac{\partial^2\mathbf{X}}{\partial s^2}\right) + \frac{\partial}{\partial s}\left(\mathscr{A}\frac{\partial\mathscr{V}}{\partial s}\mathbf{n}\right) - \mathbf{F}, \tag{3}$$

where $\mathbf{X}$ is the instantaneous location of this plate, along which a Lagrangian coordinate s is defined. m is the mass per unit length of the plate. k_b is the bending stiffness. $\boldsymbol{\tau}$ and $\mathbf{n}$ are the unit tangential and normal vectors of the body, respectively. The third term on the right-hand side of this equation stands for the mechanical stress generated by the voltage in the piezoelectric patches. Here $\mathscr{V}$ is the voltage in the circuit. $\mathscr{A}$ is the coupling coefficient determined by the material properties of the piezoelectric patches. $\mathbf{F}$ is the force density applied by the surrounding fluid to the structure. σ is the tension inside the plate. We assume that the plate is unstretchable (i.e., $|\partial\mathbf{X}/\partial s| = 1$) so that σ is determined through the inextensibility constraint [25–27]. At the bottom end of the plate ($s = 0$), $\mathbf{X} = \mathbf{X}_0$ (where $\mathbf{X}_0$ is a prescribed location) and $\partial\mathbf{X}/\partial s = (0, 1)$. At the top end of the plate ($s = L$), the bending moment, normal stress, and shear stress disappear.

For the circuit, we have

$$C\frac{\partial\mathscr{V}}{\partial t} = -\frac{1}{R}\mathscr{V} - \mathscr{A}\frac{\partial}{\partial t}\left(\frac{\partial^2\mathbf{X}}{\partial s^2}\cdot\mathbf{n}\right), \tag{4}$$

where C is the linear capacitance of the piezoelectric element and R is the resistance in the circuit. This circuit is connected with an infinitesimally small piece of the piezoelectric pair. The power extracted by plate 1 is then

$$P_1 = \frac{1}{R}\int_0^L \mathscr{V}^2 ds. \tag{5}$$

The same approach is employed to determine the dynamics of plate i ($i = 2, \ldots, N$), whose power extraction is obtained as P_i.

To normalize the problem, we choose L as the characteristic length, T as the characteristic time, ρL as the characteristic mass per unit length, and $LT^{-1}\sqrt{\rho L/C}$ as the characteristic voltage. For convenience, hereafter we use the same symbols for dimensional variables (e.g., s, t, m, $\mathbf{X}$, σ, $\mathbf{F}$, $\mathscr{V}$, and P_i) to represent their dimensionless counterparts. Subsequently, Eqs. (3) and (4) are normalized as

$$m\frac{\partial^2\mathbf{X}}{\partial t^2} = \frac{\partial}{\partial s}(\sigma\boldsymbol{\tau}) - \frac{\partial^2}{\partial s^2}\left(\kappa\frac{\partial^2\mathbf{X}}{\partial s^2}\right) + \frac{\partial}{\partial s}\left(\alpha\sqrt{\kappa}\frac{\partial\mathcal{V}}{\partial s}\mathbf{n}\right) - \mathbf{F} \tag{6}$$

and

$$\beta\frac{\partial\mathcal{V}}{\partial t} = -\mathcal{V} - \alpha\beta\sqrt{\kappa}\frac{\partial}{\partial t}\left(\frac{\partial^2\mathbf{X}}{\partial s^2}\cdot\mathbf{n}\right), \tag{7}$$

where $\alpha = \mathcal{A}/\sqrt{k_b C}$, $\beta = CR/T$, and $\kappa = k_b/(\rho L^5 T^{-2})$.

The normalized power extraction is

$$P_i = \frac{1}{\beta}\int_0^1 \mathcal{V}^2 ds. \tag{8}$$

Equations (6)–(8) are solved for each plate to find its power extraction. The time-averaged value of P_i is calculated as $\overline{P}_i = \frac{1}{T}\int_{t_0}^{t_0+T} P_i dt$, where t_0 is a time instant after the steady state has been established. Furthermore, we define the group-averaged power extraction $\overline{P}_{\text{avg}}$ in an array of N plates as $\overline{P}_{\text{avg}} \equiv \frac{1}{N}\sum_{i=1}^{N}\overline{P}_i$.

B. Numerical method

The fluid-structure interaction problem formulated in Sec. III A is solved with an immersed-boundary algorithm by relating the force density exerted by the immersed structure on the fluid [i.e., **f** in Eq. (1)] and the force density applied by the surrounding fluid to the structure [**F** in Eq. (3)] through a Dirac delta function δ. We have

$$\mathbf{f}(\mathbf{x}, t) = \int_{\Gamma} \mathbf{F}(s, t)\delta[\mathbf{X}(s, t) - \mathbf{x}]ds, \tag{9}$$

where Γ represents the structure.

The force density **F**, on the other hand, is determined via the enforcement of the no-flux and no-slip conditions at the fluid-structure interface. This is achieved by connecting the neighboring fluid and structure with a spring so that they do not drift away from each other [27,28]. Mathematically, we have

$$\mathbf{F}(s, t) = \alpha_n \int_0^t [\mathbf{U}(s, \tau) - \mathbf{V}(s, \tau)]d\tau + \beta_n[\mathbf{U}(s, t) - \mathbf{V}(s, t)], \tag{10}$$

where **V** is the structural velocity and **U** is the fluid velocity at the fluid-structure interface. Under the immersed-boundary framework, **U** is obtained from the flow velocity **u** by using the delta function as

$$\mathbf{U}(s, t) = \int_{\Omega} \mathbf{u}(\mathbf{x}, t)\delta[\mathbf{x} - \mathbf{X}(s, t)]d\mathbf{x}, \tag{11}$$

where Ω is the fluid domain. α_n and β_n are numerical parameters with sufficiently large negative values, which physically correspond to the stiffness and damping property of the spring that connects the fluid and structure. Through numerical tests, we choose $\alpha_n = -4 \times 10^5$ and $\beta_n = -50$. Their exact values have a negligible effect on the results.

IV. RESULTS

The dynamics and performance of the system are determined by the following dimensionless parameters:

(1) The configuration of the array, including the number of plates in the array N and the distance D between neighboring plates. Hereby we choose N from 2 to 5. For comparison, the case with $N = 1$ (i.e., a single plate) is also examined. The range of D is between 0.1 and 1.0. When D is larger than 1 the interaction among the plates is relatively weak. If D is too small, a refined mesh will be needed in the gap for numerical accuracy, which will significantly increase the computational effort.

(2) Mechanical properties of each plate, including its stiffness κ as well as the piezoelectric parameters α and β. Based on previous studies [19,21–23], we choose $\alpha = 0.3$ and $\beta = 0.5$. The mass per unit length of a plate is chosen to be 0.5. The range of κ is between 1 and 3. Below this range, the response is often irregular [24]. Above this range, the constructive interaction, which is the focus of this study, is not pronounced. Within this range of stiffness, the deformation is dominated by the fundamental natural mode so that the maximum lateral deformation occurs at the top end of the plate.

(3) The Reynolds number R_e, defined as $\rho L U_0/\mu$. We choose $R_e = 100$ in this study.

(4) The Keulegan-Carpenter number K_C, defined as $U_0 T/L$. In the flow condition considered here, K_C is the normalized amplitude of fluid particles divided by 2π. The range of this parameter considered here is between 0.1 and 2.

Although the numerical algorithm has been extensively validated in previous studies [23,27,29], before presenting the numerical results we conduct simulations to explore the sensitivity of the results with respect to numerical parameters to demonstrate the accuracy of the predictions. Towards this end, we create three different numerical meshes with different δx, δy, and N_B. δx and δy are the

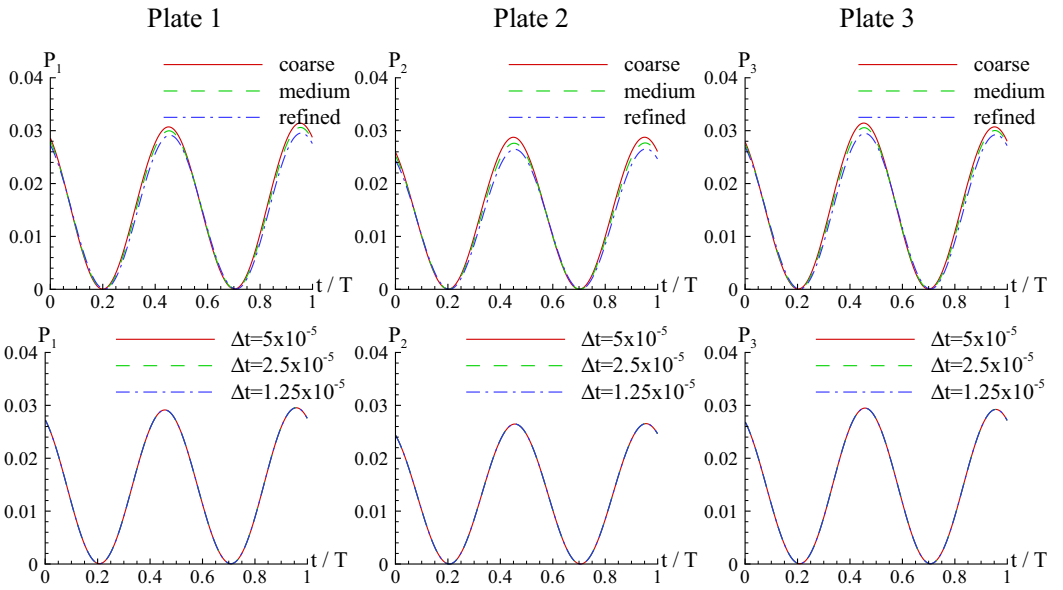

FIG. 2. Sensitivity of the power extraction P_i ($i = 1, 2, 3$) with respect to the mesh density (upper row) and time step δt (lower row). $N = 3$, $K_C = 1$, $\kappa = 1$. In the mesh density tests $\delta t = 2.5 \times 10^{-5}$. In the time step tests the refined mesh is used.

sizes of the fluidic mesh in the vicinity of the structure. N_B is the number of structural grids on a plate. The three meshes are a coarse mesh ($\delta x = \delta y = 0.033$, $N_B = 39$), a medium mesh ($\delta x = \delta y = 0.025$, $N_B = 53$), and a refined mesh ($\delta x = \delta y = 0.0167$, $N_B = 78$).

Furthermore, three different time steps, $\delta t = 5 \times 10^{-5}$, 2.5×10^{-5}, and 1.25×10^{-5}, have been adopted to show the accuracy of the time integration in the algorithm.

In Fig. 2, we plot the time histories of the power extraction P_i ($i = 1, 2, 3$) in a case with $N = 3$, $K_C = 1$, and $\kappa = 1$ with different meshes and time steps within the 19th period. All the results in this section are obtained after the steady state is established. It usually takes 10–20 periods. For simplicity, in the figures of time histories or snapshots presented in this section we shift the starting time to $t = 0$.

Based on Fig. 2, it is clear that the results are not sensitive to the choice of the computational mesh (see the upper row). The effect of the time step is even less significant—the time histories of P_i obtained with different time steps shown in the lower row in Fig. 2 are graphically indistinguishable from each other.

In addition to these tests, we have also checked the effect of the size of the computational domain by using other domain sizes (e.g., $30L \times 30L$). The impact was found to be negligibly small.

To characterize the dynamic response and energy-harvesting capacity of the system, we will document the amplitude of vibration at the top end in the horizontal direction and the time-averaged power extraction ($\overline{P}_i$ and $\overline{P}_{\text{avg}}$). Hereby the amplitude of the top end of plate i is defined as $a_i = (x_{t_{\max}} - x_{t_{\min}})/2$, where $x_{t_{\max}}$ and $x_{t_{\min}}$ are the maximum and minimum x locations of the top end of this plate, respectively. The average value of a_i within an array, a_{avg}, is defined as $a_{\text{avg}} \equiv \frac{1}{N}\sum_{i=1}^{N} a_i$, the group-averaged vibration amplitude at the top ends.

To quantitatively study the effect of hydrodynamic interactions among the plates in an array, we use two dimensionless parameters, A_a and A_P, to show the comparison between the plates in an array and a single stand-alone plate. A_a, the amplitude amplification factor, is defined as a_{avg}/a_0, where a_0 is the amplitude of the end of a single stand-alone plate in horizontal direction under the same

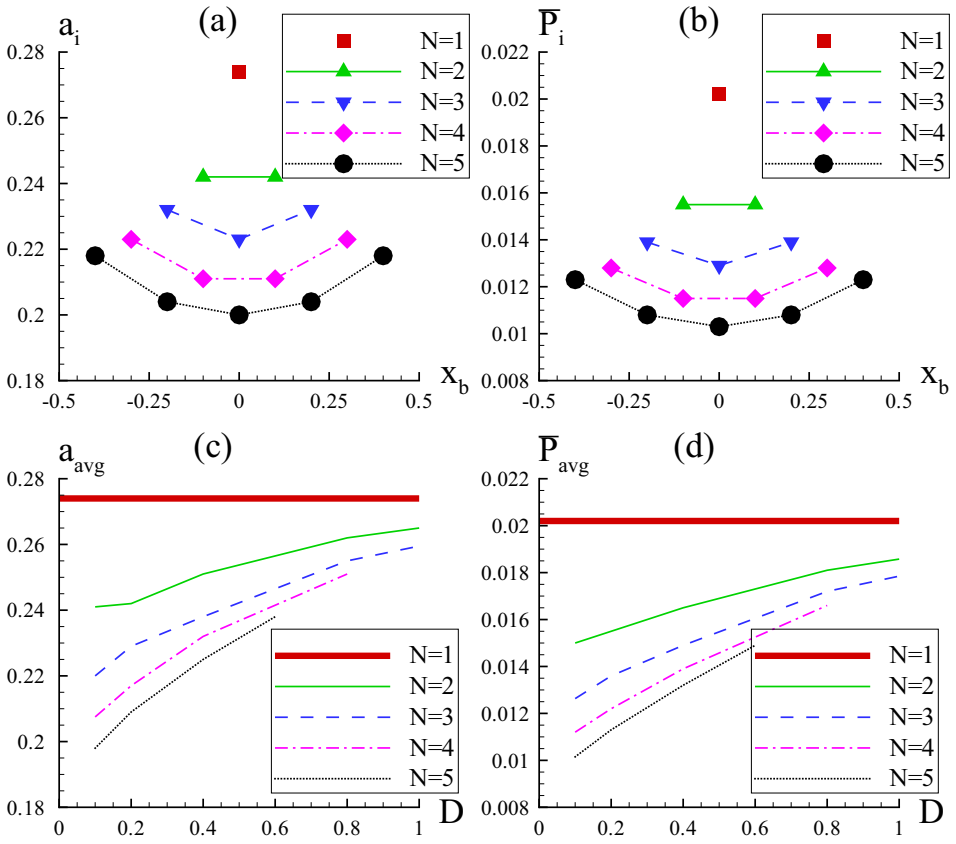

FIG. 3. (a) Amplitude of the top end a_i and (b) time-averaged power extraction capacity P_i of a plate whose bottom end locates at $x = x_b$ within different array configurations ($D = 0.2$). (c) and (d) The group-averaged values of a (a_{avg}) and P ($\overline{P}_{\text{avg}}$) within an array as functions of D. $\kappa = 1$, $K_C = 1$.

structural and hydrodynamic conditions. Similarly, the power amplification factor A_P is defined as $\overline{P}_{\text{avg}}/\overline{P}_0$, where $\overline{P}_0$ is the time-averaged power extraction of a single plate.

A. Destructive and constructive interactions

By definition, destructive interaction refers to the scenario when $A_a < 1$ or $A_P < 1$. In this scenario, the hydrodynamic interaction among the plates in an array reduces the group-averaged deformation and/or the power extraction. In contrast, when constructive interaction occurs the group-averaged deformation and the power extraction are increased so that A_a and A_P are larger than 1.

A typical case of destructive interaction in an array is displayed in Fig. 3. In this case the plate stiffness $\kappa = 1$ and the Keulegan-Carpenter number $K_C = 1$. The number of plates in the array (N) ranges from one to five. According to Fig. 3(a), at $D = 0.2$ when $N \geqslant 2$ the amplitudes of deformation of the plates in an array are all below that of a single plate ($N = 1$). In addition, within an array the plates near the border deform more than those in the middle; in fact, the one located at the center has the least deformation in the bunch. Similar trends are observed in the behavior of the time-averaged power extraction [Fig. 3(b)]. Another notable phenomenon in these figures is that as N increases, the group-averaged deformation amplitude (a_{avg}) and power extraction ($\overline{P}_{\text{avg}}$) decrease. This is confirmed in Fig. 5(a), where the dependencies of A_a and A_P upon N are plotted.

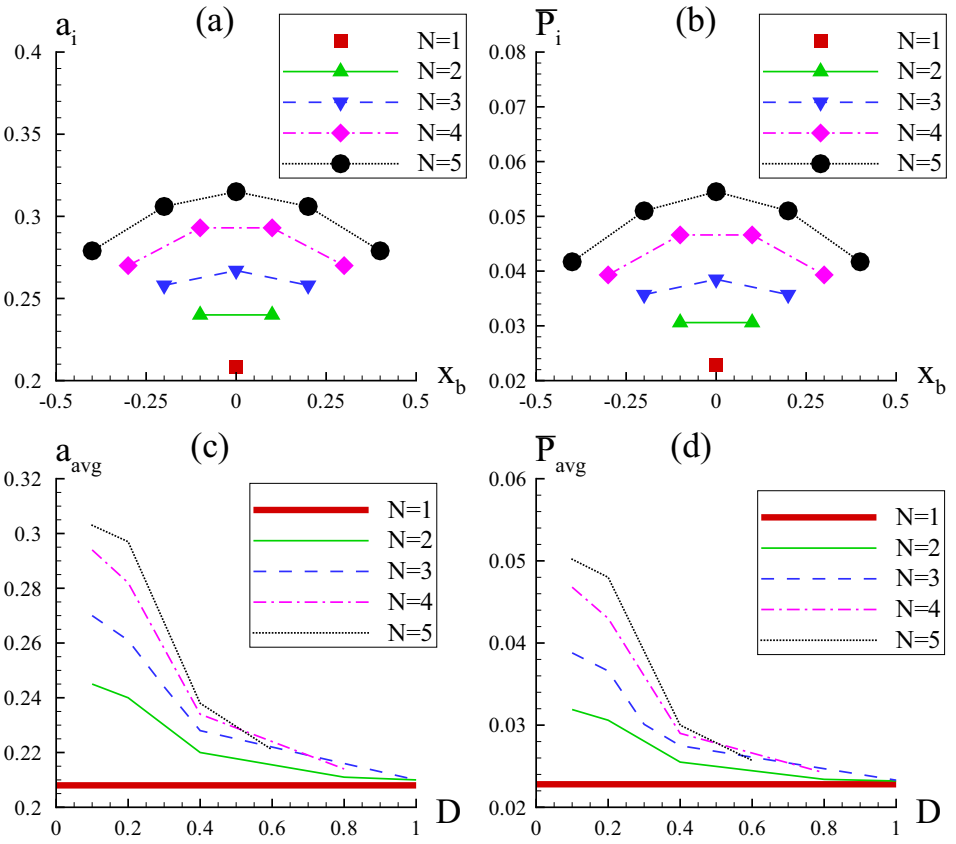

FIG. 4. Same as Fig. 3 except that $\kappa = 2$ and $K_C = 0.5$.

In Figs. 3(c) and 3(d) we plot the dependencies of a_{avg} and $\overline{P}_{\text{avg}}$ upon D, the distance between neighboring plates. Both decrease almost monotonically when D is reduced. The exception occurs at the case when $N = 2$. In this case when D drops below 0.2 there is a tendency for a_{avg} to plateau. However, due to the limitation of the computational mesh it is difficult to further reduce the value of D, so the exact behavior of the system when D is very small has not been investigated.

Figure 4 demonstrates a typical case of constructive interaction among plates in an array. In comparison with the previous case, the most important change in physical parameters is that the plate stiffness is increased from 1 to 2. Although the Keulegan-Carpenter number has also been changed (from 1 to 0.5), it is not the determining factor. Indeed, even if K_C stays at 1, when κ is 2 we still see constructive interactions (see, e.g., Fig. 13).

According to Figs. 4(a) and 4(b), in this case the deformation and power extraction of a plate in an array surpass those of a single plate. Moreover, the plates near the center in the formation deforms more than those near the border, with the maximum deformation occurring right at the center. Similar to the destructive case, the effect of constructive interaction becomes more pronounced when the number of plates in an array increases [see Fig. 5(b)]. For example, when $N = 2$ the values of A_a and A_P are 1.15 and 1.34, respectively. When $N = 5$, on the other hand, these values are increased to 1.43 and 2.10, indicating that by using an array of five plates the average energy-harvesting performance of each plate is increased by 110%. The implication is that the performance of the system can be significantly improved by using large arrays in which the individual plates interact constructively with their neighbors.

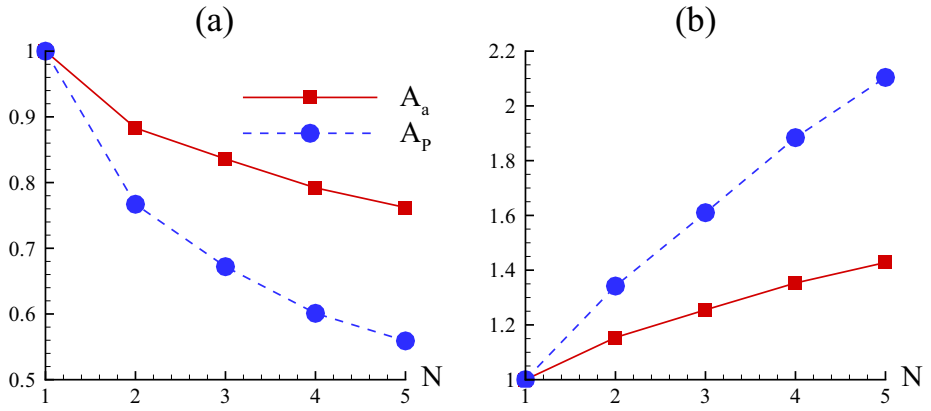

FIG. 5. Amplification factors A_a and A_P at different array size N. (a) $\kappa = 1$, $K_C = 1$; (b) $\kappa = 2$ and $K_C = 0.5$. $D = 0.2$.

Figures 4(b) and 4(c) show the effect of the gap size D on a_{avg} and $\overline{P}_{\text{avg}}$. When D is decreased, both a_{avg} and $\overline{P}_{\text{avg}}$ increase until the neighboring plates are too close to each other ($D < 0.2$), when the slopes of these curves start to decrease. Again, with the current method it is not possible to study the cases in which D is very small.

The plate stiffness κ is a key parameter that plays a critical role in determining the (destructive versus constructive) nature of the hydrodynamic interaction inside an array. For example, in Fig. 6 we plot the dependencies of A_a and A_P upon κ with the other parameters fixed as $D = 0.2$ and $K_C = 0.5$. Under these conditions constructive interaction is achieved when κ is in the range between 1.55 and 2.75, regardless of how many plates are in the array (although the effect is more pronounced when N increases). Another notable phenomenon is that when κ is large (e.g., $\kappa = 3$), there could be a symmetry-breaking effect that disturbs the symmetry in the longitudinal direction. This effect depends not only on κ but also on other parameters such as D and K_C. An example is shown in Fig. 7, where we consider the case when $\kappa = 3$ and $K_C = 0.4$. Based on this figure, it is seen that the responses of the plates are not symmetric in the x direction.

B. Underlying physical mechanisms

As indicated in Fig. 6, the plate stiffness κ plays a critical role in determining the interaction mode between neighboring plates. To investigate the underlying physics of destructive and constructive interactions, we choose cases with three typical values of κ (1, 2, and 3) to examine the differences in the features of the surrounding flow fields in destructive and constructive interaction scenarios.

For clarity, we consider a single stand-alone plate. As the interaction between a plate and its surrounding flow field is closely associated with the relative motion between it and the flow, in Fig. 8 we plot time histories of the horizontal velocity at the top end of such a plate (u_{xt}) together with that of the background flow (U) in three cases with $\kappa = 1$, 2, and 3 within a period. According to Fig. 8(a), when the plate is soft ($\kappa = 1$), u_{xt} and U are in phase with each other over the whole period. The phase difference between the two estimated by using the peaks of the two curves is only about 1°. Although the difference between u_{xt} and U suggests that this is not a pure feathering scenario, the relative speed between the top end and the background flow in this case is small so that separation and vortex generation from the top end are negligibly weak [Fig. 9(a)]. In this scenario the effect of this plate on its neighbor downstream is mostly blocking—it weakens both the speed and the pressure gradient from the background flow on the neighboring plate. This effect is particularly strong for plates in the middle of an array since these plates are blocked during the whole period by their neighbors on both sides, whereas the plates on the borders are only blocked

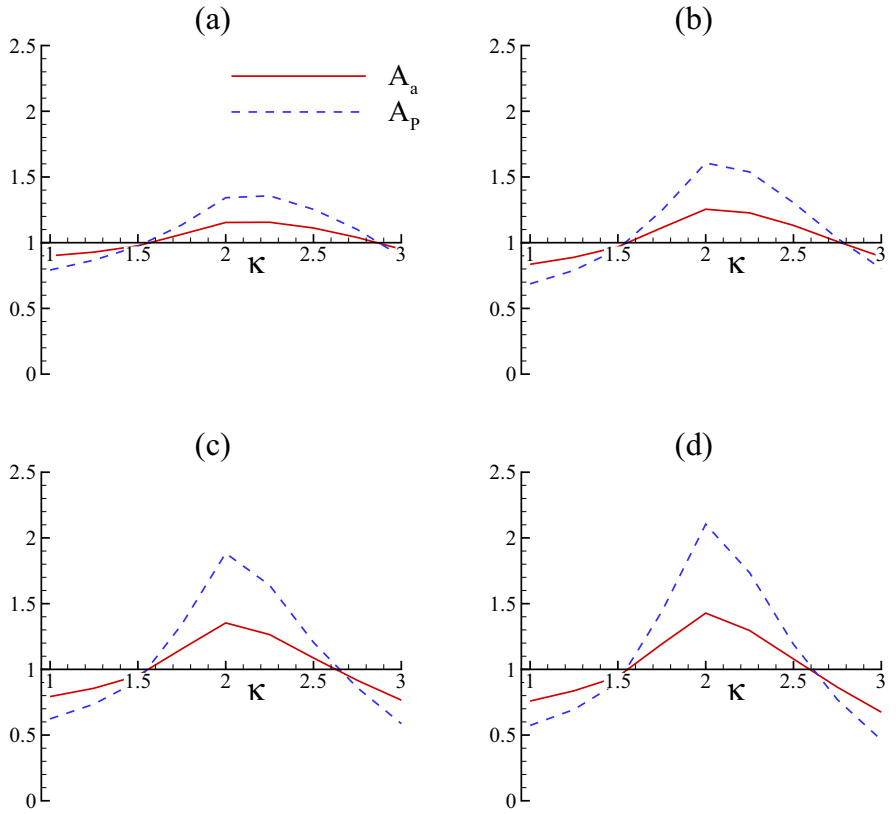

FIG. 6. Dependencies of amplification factors A_a and A_P on κ at (a) $N = 2$, (b) $N = 3$, (c) $N = 4$, and (d) $N = 5$. $D = 0.2$, $K_C = 0.5$.

during half of a period since they only have a neighbor on one side. This explains the trend that the destructive interaction effect is more pronounced for plates in the middle of a formation, discussed in Sec. IV A.

The next case we consider is the one with $\kappa = 2$ and $K_C = 0.5$, in which constructive interaction has been found (see Sec. IV A). In this case there is a small phase difference (around 17°) between the motion of the top end of the plate and the background flow [Fig. 8(b)]. However, in comparison with the case in which $\kappa = 1$, in the current case there is an increased difference between the amplitudes of u_{xt} and U so that the relative motion between the plate and the flow is also increased, leading to more pronounced vortex shedding from the top end. As shown in Figs. 9(b) and. 10(a), at the beginning of the period ($t = 0$), the background flow speed is zero. The plate tends to sweep back to the right due to its own bending stiffness. After this moment both the background flow speed U and the speed of the top end of the plate u_{xt} are in the $+x$ direction. In this case the bending stiffness is sufficiently large so that the top end of the plate moves faster than the background flow. It creates a counterclockwise vortex [marked as vortex "V" in the sketch in Fig. 10(a)]. After this vortex is generated, it grows in strength and sheds to the left side of the plate [see the snapshots at $t = 8/T$ and $t = T/4$ in Fig. 10(a)].

To examine the effect of the aforementioned vortex shedding process on the dynamics of an array of plates, we use a formation of three plates with $\kappa = 2$ and $K_C = 0.5$ as an example. The surrounding flow fields in this case are shown in Fig. 11. To clearly show the vorticity field, we choose $D = 0.4$. Similar to the single-plate case, each plate in the array generates a counterclockwise vortex from its top end at the beginning of the period. These vortices are marked as "V1," "V2," and "V3"

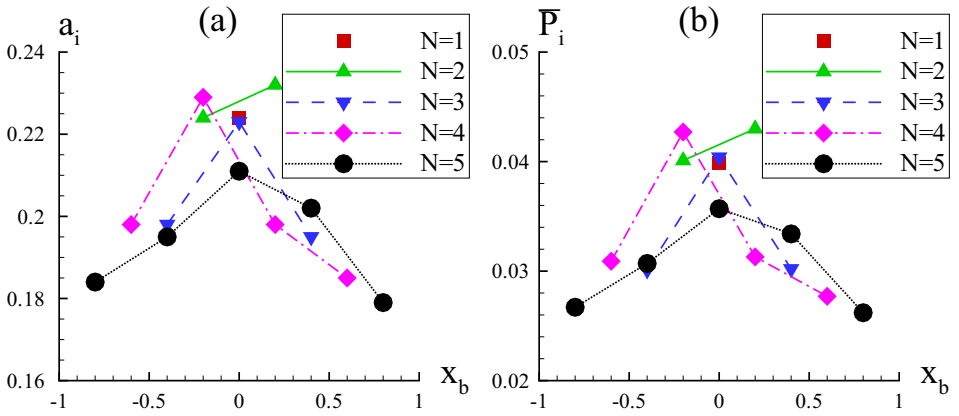

FIG. 7. (a) Amplitude of the top end a_i and (b) time-averaged power extraction capacity $\overline{P}_i$ of a plate whose bottom end locates at x_b within different array configurations. $\kappa = 3$, $K_C = 0.5$, $D = 0.4$.

in the sketches shown in Fig. 11, corresponding to the vortex shed from plate 1 (the left plate), the one from plate 2 (the middle plate), and the one from plate 3 (the right plate).

Vortices induce areas of low pressure so that they could impose suction force on solid surfaces nearby. In the case shown in Fig. 11, during the first half of the period, vortex V2 creates a rightward force near the top of plate 1. Similarly, vortex V3 also generates a rightward force on plate 2. These forces are in the same direction as the motion of these two plates so that they pump mechanical energy into these plates and enhance their vibrations. Within the time slot shown in the figure, there is no such additional energy source for plate 3. During the second half of the period, however, the direction of the flow is reversed so that plate 3 can harvest energy from the vortex shed from the top end of plate 2. Meanwhile, plate 2 can harvest energy from the wake of plate 1. This is the physical mechanism behind the phenomenon of constructive interaction. Moreover, since plate 2 is able to harvest wake energy within the whole period, whereas plate 1 and plate 3 are only able to do so during half of the period, plate 2 should deform more than the other two. This is consistent with the results shown in Fig. 4.

Finally, we consider the case when $\kappa = 3$ and $K_C = 0.5$ in Figs. 8(c), 9(c), and 10(b). As indicated in Fig. 8(c), in this case the phase difference between u_{xt} and U is significant (about 48°); indeed, during part of the period [$t \in (0.33, 0.5)$ and $t \in (0.84, 1.0)$] these two are in opposite directions. Thus there is considerable relative motion between the plate and the background flow, leading to the following consequences:

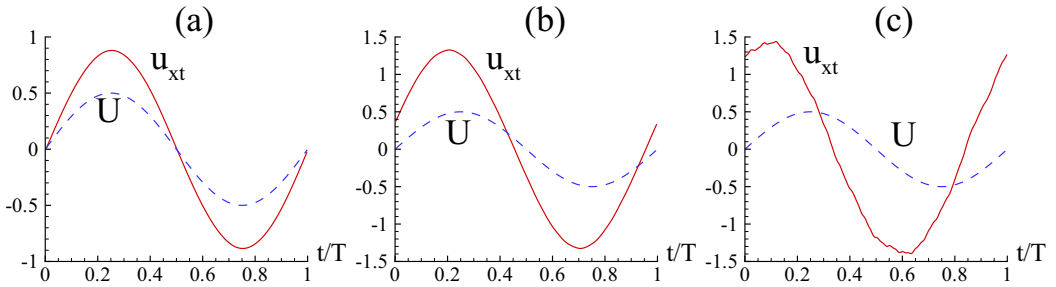

FIG. 8. Horizontal velocity at the top end of a single plate (u_{xt}) and the background flow velocity (u_f) during a period with (a) $\kappa = 1$, (b) $\kappa = 2$, and (c) $\kappa = 3$. $N = 1$, $K_C = 0.5$.

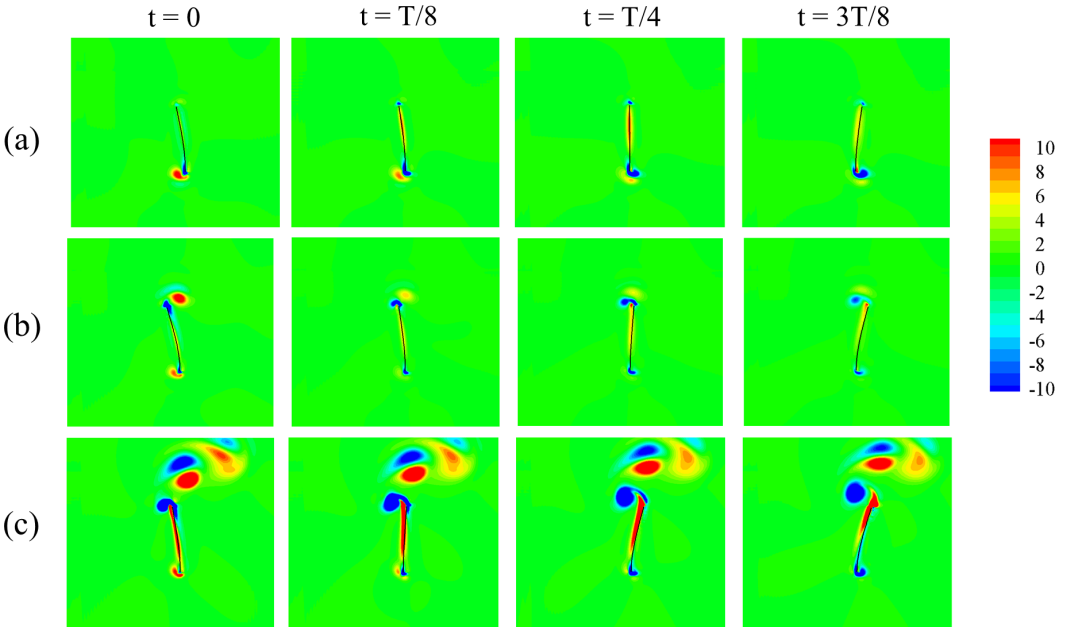

FIG. 9. Snapshots of the flow field around the plates visualized through vorticity contour during half a period for (a) $\kappa = 1$, (b) $\kappa = 2$, and (c) $\kappa = 3$. $N = 1$, $K_C = 0.5$.

(1) The strength of vortices shed from the top end is enhanced [Fig. 9(c)]. This is supposed to enhance the wake energy recovery mechanism. However, in this case the body motion and the load from the vortex shed from its neighbor is not well synchronized in comparison with the case when $\kappa = 2$. This can be seen in Fig. 10 by comparing the plots in (a) and (b) at $t = 3T/8$. Subsequently the work done by the vortex-induced load could be negative during part of the period. It will reduce the wake energy recovery mechanism.

(2) Another consequence of the increased relative motion between the plate and the background flow (especially when they are in opposite directions) is the significant increase in the shielding mechanism due to the disturbance from the plate.

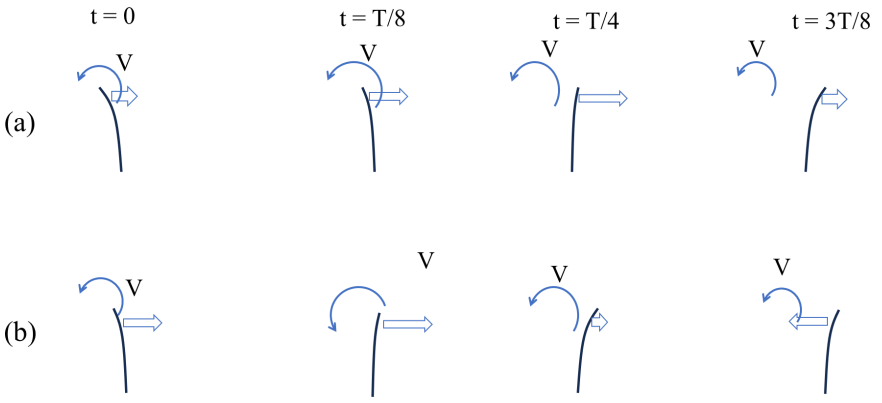

FIG. 10. Schematic illustrations of plate deformation and vortex generation at (a) $\kappa = 2$ [the case shown in Fig. 9(b)] and (b) $\kappa = 3$ [the case shown in Fig. 9(c)]. The arrows indicate the direction and (qualitatively) the speed of horizontal motion at the top end.

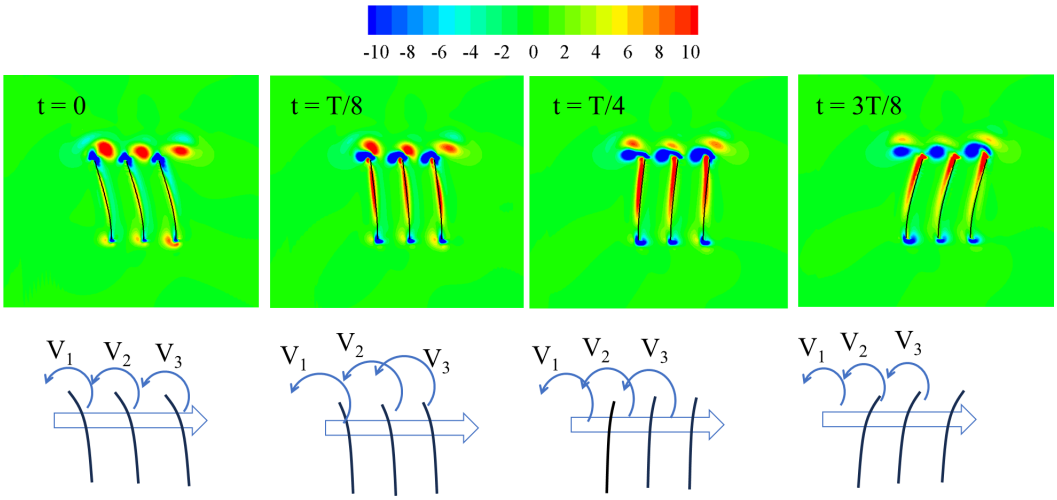

FIG. 11. Upper row: Snapshots of the flow field around a formation of three plates visualized through vorticity contour during half a period for $\kappa = 2$, $K_C = 0.5$, and $D = 0.4$. Lower row: Schematic illustrations of the plate deformation and vortex generation. The arrows indicate the direction of horizontal motion at the top ends.

(3) When the vortices are sufficiently strong, the interactions among them and their interactions with the flexible structure may trigger symmetry-breaking instabilities, leading to nonsymmetric behavior as shown in Fig. 7.

Considering these effects, the exact interaction mode (destructive or constructive) is determined by the dominant one between the wake energy recovery mechanism and the shielding mechanism. It depends not only on the stiffness κ, but also on other physical parameters such as D and K_C (see Sec. IV C).

To conclude, in terms of the hydrodynamic interaction among plates in an array, there exist two competing physical mechanisms. One of them is the shielding mechanism, referring to the effect that due to the presence of an upstream plate, the impact of the incoming flow on the downstream plate is reduced so that the deformation of this plate is diminished. The other one is the energy recovery from the wake of a neighboring plate (i.e., the vortices shed from the top end of this plate).

For example, considering the cases shown in Fig. 6, where $D = 0.2$ and $K_C = 0.5$, in the soft plate case ($\kappa = 1$), the vorticity generation from the top ends of the plates is weak, so the energy recovery mechanism is insignificant in comparison with the shielding mechanism. The net effect is thus the destructive interaction. In the medium-softness plate ($\kappa = 2$), with vortex shedding from the top ends of the plates the energy recovery mechanism surpasses the shielding mechanism, leading to the constructive interaction. When the plates are stiff (e.g., $\kappa = 3$), the energy recovery mechanism is overwhelmed by the shielding mechanism. This explains the tendency shown in Fig. 6 that the amplification factors decline when $\kappa >\sim 2.3$.

As suggested by Fig. 8, the phase difference between u_{xt} and U is closely related to constructive interaction; for it to occur the value of this difference cannot be too large. This parameter is affected not only by κ, but also by the flow conditions such as the Keulegan-Carpenter number K_C. For instance, in the case when $\kappa = 2$, if K_C is increased from 0.05 to 0.2, this phase difference becomes 37°, and consequently the interaction mode switches from constructive to destructive (when $N = 2$ and $D = 0.2$, the values of A_a and A_P are 0.97 and 0.91, respectively). Physically, the phase difference between u_{xt} and U depends on the following factors:

(1) *The phase of the hydrodynamic load on a plate*: According to the Morison equation [30], this load includes two parts: a viscous drag that is in phase with the background flow speed, and an added-mass load that is in phase with the background flow acceleration. The relative strength

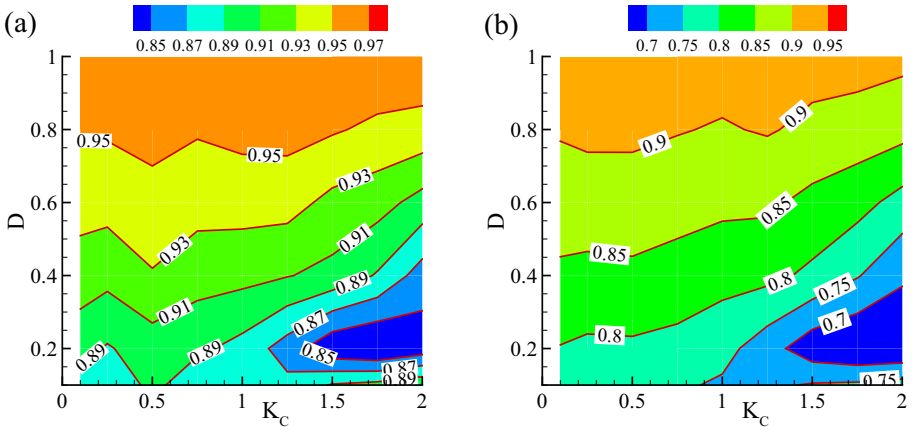

FIG. 12. Amplification factors A_a (a) and A_P (b) at various combinations of D and K_C. $N = 2$, $\kappa = 1$.

of each effect depends on parameters such as the Keulegan-Carpenter number and the Reynolds number.

(2) *The frequency ratio*: This is the ratio between the background flow frequency and the frequency of the fundamental natural mode of the plate. The natural frequencies of the plate depend on its bending stiffness κ and mass per unit length m. With m fixed at 0.5, flow-structure resonance is achieved when κ is around 2.5 according to numerical tests [24].

The effects of the phase difference between u_{xt} and U on the wake energy recovery mechanism are summarized in the following: (1) If the phase difference is small, the relative motion between the top ends of the plates and the incoming flow is small so that the vortices generated there are weak. In this scenario there is not much energy to be harvested in the wake. (2) If the phase difference is adequate, the top-end vortices are sufficiently strong. Meanwhile, the suction forces generated by these vortices on neighboring plates are more or less in phase with their motions so that they pump energy into the plates and significant wake energy recovery is achieved. (3) If the phase difference is too large, the top-end vortices are further strengthened. However, there is also an increased phase lag between the suction forces and motions of the plates so that the energy recovery mechanism is diminished. In addition, when the relative motion between the plates and the flow is large, the incoming flow field is severely disturbed by the plates so that the shielding effect is strong. With these two effects combined, in these cases the shielding effect is often dominant.

In addition, the separation D is another important physical parameter in determining the interaction mode. In our case the Reynolds number and the mass per unit length are both fixed. The effects of K_C and D are considered in detail in Sec. IV C.

C. Parametric studies: Effects of K_C and D

For further insight into the occurrence of constructive interaction at different combinations of physical parameters, we conduct additional simulations to examine the constructive and destructive effects, characterized by the amplification factors A_a and A_P, in the interaction among piezoelectric plates in an array. Towards this end, we will fix N at 2 (according to the results presented in Secs. IV A and IV B, N plays little role in determining the nature of the interaction, although it does affect the exact values of the amplification factors). Three values of κ are chosen, a small one at $\kappa = 1$, an intermediate one at $\kappa = 2$, and a large one at $\kappa = 3$.

Figure 12 displays the values of A_a and A_P at various D and K_C when $\kappa = 1$. At this value of κ the energy recovery mechanism is negligible so that destructive interaction (i.e., $A_a < 1$, $A_P < 1$) dominates within the whole range of parameters. This interaction mode is attributed to the blocking of flow and pressure gradient by the upstream plate. It is particularly strong when D is small and K_C is large.

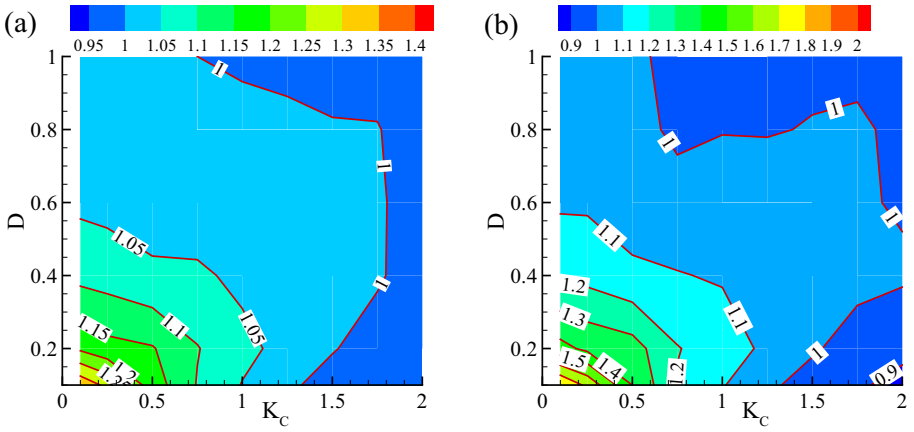

FIG. 13. Amplification factors A_a (a) and A_P (b) at various combinations of D and K_C. $N = 2$, $\kappa = 2$.

When κ rises to 2, constructive interaction becomes the dominant interaction mode (see Fig. 13). In fact, only when K_C is large there are relatively small regions in the parametric space corresponding to destructive interaction. Within the range of parameters we consider, the maximum value of A_a is 1.34 and the maximum value of A_P is 1.80. Both are achieved at $D = 0.1$ and $K_C = 0.1$.

Finally, in Fig. 14 we plot the dependencies of A_a and A_P upon D and K_C when $\kappa = 3$. In comparison with the case when $\kappa = 2$, the size of the area corresponding to constructive interaction in the parametric space is reduced. Meanwhile, the peak values of A_a and A_P are reduced to 1.14 and 1.31, respectively. Both of these values occur when $D = 0.4$ and $K_C = 0.25$.

In general, these studies show that intermediate plate stiffness is most beneficial in achieving constructive interactions.

V. CONCLUSIONS

Based on the immersed-boundary framework, a numerical model has been created by combining a Navier-Stokes fluid solver with a structural model and a resister-capacitor model of a resistive circuit to simulate the dynamics and energyharvesting capacity of a group of piezoelectric plates in oscillatory cross flow. These plates are fixed at one end and free at the other.

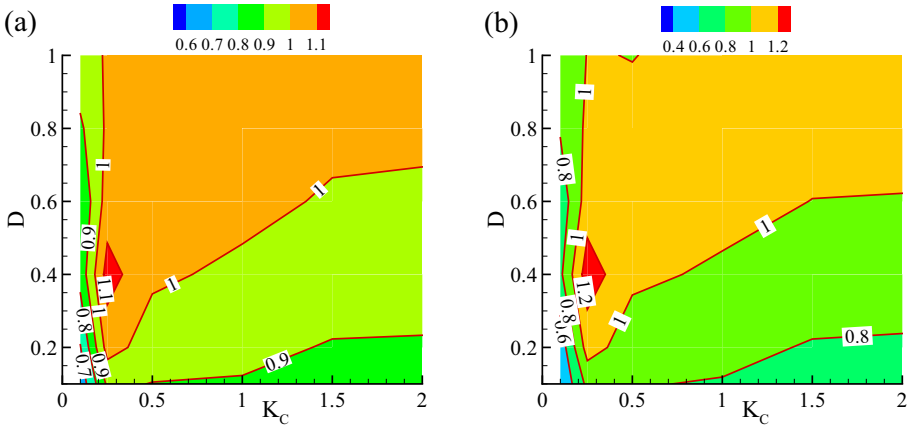

FIG. 14. Amplification factors A_a (a) and A_P (b) at various combinations of D and K_C. $N = 2$, $\kappa = 3$.

Simulations have been conducted to study the performance of this system in different conditions, including the configuration of the array (i.e., the number of plates in the array and the distance between neighboring plates), the bending stiffness of a plate, and the frequency/strength of the background oscillatory flow. We are particularly interested in determining the underlying mechanisms of destructive and constructive interactions among the plates in an array as well as the conditions for constructive interaction to occur.

Two counteractive physical mechanisms have been identified. The first one is the shielding mechanism, corresponding to the reduction of flow speed and pressure gradient of the ambient flow by upstream plates. The other one is the energy recovery mechanism. When this happens, a plate is able to extract energy from the vortices shed from its neighbors so that its deformation and energy-harvesting capability are enhanced. In cases dominated by the first mechanism, the interactions among the array are destructive so that the group-averaged deformation and power extraction are smaller than those of a stand-alone plate. On the other hand, when the second mechanism dominates, the interaction is constructive, which improves the energy-harvesting performance of the system. In both scenarios, the effect becomes more pronounced as the number of plates in a formation is increased.

An important physical parameter that determines the occurrence of destructive and constructive interactions is the plate stiffness. When a plate is too soft, it features under the impact of the flow and subsequently little vorticity is generated from its free end. It is thus not possible for its neighboring plates to recover energy from its wake so that the interaction is destructive. When a plate is too stiff, it does create strong vortices from its free end for energy recovery. However, its shielding effect is also strong and it may outweigh the energy recovery effect in many cases. Therefore, to achieve constructive interaction the best option is intermediate plate stiffness. The basic requirements for constructive interaction are (1) the plates are not too soft to avoid feathering response and (2) the phase difference between the vibration of the plates and the background flow is relatively small. Other parameters, such as the Keulegan-Carpenter number and the separation between neighboring plates, also play a role.

The current study is based on an idealized scenario in which the flow field resembles the flow caused by a shallow-water wave whose wave length is much larger than the length scale of the system. The flow fields related to more general wave conditions are more complicated since there is a vertical flow component as well as variations of flow velocity in the horizontal direction. Nevertheless, the physical mechanisms identified in the present study are universal so that they can be applied for qualitatively understanding the fluid-structure interaction problems involved in those scenarios.

Another issue that needs to be investigated in future studies is the behavior of the system when N is large. The current results suggest that the constructive interaction effect increases monotonically with N when N is in the range between 1 and 5. There is no knowledge about this effect above this range. The difficulty of such study lies mostly on the computational effort since larger computational domains, and subsequently more grids in the fluid domain, are necessary.

[1] C. Wang, F. Tang, and X. Zhang, Fluid-structure interaction of bio-inspired flexible slender structures: A review of selected topics, Bioinspir. Biomim. **17**, 041002 (2022).

[2] B. Connell and D. Yue, Flapping dynamics of a flag in uniform stream, J. Fluid Mech. **581**, 33 (2007).

[3] S. Alben and M. Shelley, Flapping states of a flag in an inviscid fluid: Bistability and the transition to chaos, Phys. Rev. Lett. **100**, 074301 (2008).

[4] S. Banerjee, B. Connell, and D. Yue, Three-dimensional effects on flag flapping dynamics, J. Fluid Mech. **783**, 103 (2015).

[5] D. Kim, J. Cosse, C. Cerdeira, and M. Gharib, Flapping dynamics of an inverted flag, J. Fluid Mech. **736**, R1 (2013).

[6] X. Wang, S. Alben, C. Li, and Y. Young, Stability and scalability of piezoelectric flags, Phys. Fluids **28**, 023601 (2016).
[7] S. Lim and S. Park, Numerical analysis of energy harvesting system including an inclined inverted flag, Phys. Fluids **34**, 013601 (2022).
[8] X. Zhang, G. He, and X. Zhang, Fluid-structure interactins of single and dual wall-mounted 2D flexible filaments in a laminar boundary layer, J. Fluids Struct. **92**, 102787 (2020).
[9] X. Zhang, Y. Li, and X. Zhang, Dynamic interactions of muliple wall-mounted flexible plates in a laminar boundary layer, Front. Phys. **10**, 881966 (2022).
[10] X. Xie, Q. Wang, and N. Wu, Potential of a piezoelectric energy harvester from sea waves, J. Sound Vib. **333**, 1421 (2014).
[11] Y. Cui, H. Wang, M. Li, and K. Sun, Simulation of wave energy harvesting by piezoelectric seaweed, IOP Conf. Ser: Mater. Sci. Eng. **250**, 012022 (2017).
[12] N. Wang, J. Zou, Y. Yang, X. Li, Y. Guo, C. Jiang, X. Jia, and X. Cao, Kelp-inspired biomimetic triboelectric nanogenerator boosts wave energy harvesting, Nano Energy **55**, 541 (2019).
[13] Y. Wang, X. Liu, Y. Wang, H. Wang, H. Wang, S. Zhang, T. Zhao, M. Xu, and Z. Wang, Flexible seaweed-like triboelectric nanogenerator as a wave energy harvester powering marine internet of things, ACS Nano **15**, 15700 (2021).
[14] D. Wang and H. Ko, Piezoelectric energy harvesting from flow-induced vibration, J. Micromech. Microeng. **20**, 025019 (2010).
[15] H. Akaydin, N. Elvin, and Y. Andreopoulos, Energy harvesting from highly unsteady fluid flows using piezoelectric materials, J. Intell. Mater. Syst. Struct. **21**, 1263 (2010).
[16] M. Safaei, H. Sodano, and S. Anton, A review of energy harvesting using piezoelectric materials: State-of-the-art a decade later (2008–2018), Smart Mater. Struct. **28**, 113001 (2019).
[17] D. Akcabay and Y. Young, Hydroelastic response and energy harvesting potential of flexible piezoelectric beams in viscous flow, Phys. Fluids **24**, 054106 (2012).
[18] O. Doare and S. Michelin, Piezoelectric coupling in energy-harvesting fluttering flexible plates: Linear stability analysis and conversion efficiency, J. Fluids Struct. **27**, 1357 (2013).
[19] S. Michelin and O. Doare, Energy harvesting efficiency of piezoelectric flags in axial flows, J. Fluid Mech. **714**, 489 (2013).
[20] Y. Xia, S. Michelin, and O. Doare, Fluid-solid-electric lock-in of energy harvesting piezoelectric flags, Phys. Rev. Appl. **3**, 014009 (2015).
[21] K. Shoele and R. Mittal, Energy harvesting by flow-induced flutter in a simple model of an inverted piezoelectric flag, J. Fluid Mech. **790**, 582 (2016).
[22] S. Mazharmanesh, J. Young, F. Tian, S. Ravi, and J. Lai, Energy harvesting of inverted piezoelectric flags in an oscillating flow, J. Fluids Struct. **115**, 103762 (2022).
[23] X. Bi, C. Wang, Q. Zhu, and H. Tang, Energy harvesting using an inverted piezohydroelastic flag with resistor-inductor-capacitor circuit, J. Fluid Mech. **975**, A49 (2023).
[24] Q. Zhu and Q. Xiao, Dynamics of seaweed-inspired piezoelectric plates for energy harvesting from oscillatory cross flow, Bioinspir. Biomim. **19**, 046004 (2024).
[25] A. Tornberg and M. Shelley, Simulating the dynamics and interactions of flexible fibers in Stokes flows, J. Comput. Phys. **196**, 8 (2004).
[26] W. Huang, S. J. Shin, and H. Sung, Simulation of flexible filaments in a uniform flow by the immersed boundary method, J. Comput. Phys. **226**, 2206 (2007).
[27] K. Shoele and Q. Zhu, Leading edge strengthening and the propulsion performance of flexible ray fins, J. Fluid Mech. **693**, 402 (2012).
[28] D. Goldstein, R. Handler, and L. Sirovich, Modelling a no-slip flow boundary with an external force field, J. Comput. Phys. **105**, 354 (1993).
[29] K. Shoele and Q. Zhu, Performance of a wing with nonuniform flexibility in hovering flight, Phys. Fluids **25**, 041901 (2013).
[30] O. Faltinsen, *Sea Loads on Ships and Offshore Structures* (Cambridge University Press, Cambridge, UK, 1990).